Spin-orbit coupling and electron scattering in high-quality $InSb_{1-x}As_x$ quantum wells

S. Metti,[1,2] C. Thomas,[3,2] D. Xiao,[3,2] and M. J. Manfra[3,2,1,4,5,*]

[1]*Elmore Family School of Electrical and Computer Engineering, Purdue University, West Lafayette, Indiana 47907, USA*
[2]*Birck Nanotechnology Center, Purdue University, West Lafayette, Indiana 47907, USA*
[3]*Department of Physics and Astronomy, Purdue University, West Lafayette, Indiana 47907, USA*
[4]*School of Materials Engineering, Purdue University, West Lafayette, Indiana 47907, USA*
[5]*Microsoft Quantum Lab West Lafayette, West Lafayette, Indiana 47907, USA*

(Received 30 June 2022; revised 1 September 2022; accepted 28 September 2022; published 17 October 2022)

$InSb_{1-x}As_x$ is a promising material system for exploration of topological superconductivity in hybrid superconductor/semiconductor devices due to its large effective *g*-factor and enhanced spin-orbit coupling when compared to binary InSb and InAs. Much remains to be understood concerning the fundamental properties of the two-dimensional electron gas (2DEG) in InSbAs quantum wells. We report on the electrical properties of a series of 30 nm $InSb_{1-x}As_x$ quantum wells grown 40 nm below the surface with three different arsenic mole fractions, $x = 0.05$, 0.13, and 0.19. The dependencies of mobility on 2DEG density and arsenic mole fraction are analyzed. For the $x = 0.05$ sample, the 2DEG displays a peak mobility $\mu = 2.4 \times 10^5$ cm^2/Vs at a density of $n = 2.5 \times 10^{11}$ cm^{-2}. High mobility, small effective mass, and strong spin-orbit coupling result in beating in the Shubnikov de Haas oscillations at low magnetic field. Fourier analysis of the Shubnikov de Haas oscillations facilitates extraction of the Rashba spin-orbit parameter α as a function of 2DEG density and quantum well mole fraction. For $x = 0.19$ at $n = 3.1 \times 10^{11}$ cm $^{-2}$, $\alpha \approx 300$ meVÅ, among the highest reported values in III-V materials.

DOI: 10.1103/PhysRevB.106.165304

I. INTRODUCTION

Small band gap zinc-blende III-V semiconductors (such as InAs and InSb) are the subject of renewed interest as they may be utilized as a platform to explore topological superconductivity. Strong spin-orbit coupling (SOC) and proximity-induced superconductivity from a parent *s*-wave superconductor are key ingredients needed to realize a topological phase [1–11]. Gate-controlled SOC is of fundamental and practical interest. The ability to externally manipulate the strength of SOC in a 2DEG facilitates realization of spin dependent devices, such as the spin field effect transistor [12].

The ternary compound $InSb_{1-x}As_x$ is appealing compared to InSb and InAs because it is predicted to have a higher Rashba SOC parameter α [8,13–15]. The increase in SOC with arsenic mole fraction in $InSb_{1-x}As_x$ has been measured in nanowires [16] and recently in a surface 2DEG [8,11]. Here, we focus on 30 nm quantum wells buried under a 40 nm $In_{0.88}Al_{0.12}Sb$ top barrier. Arsenic mole fractions of $x = 0.05$, $x = 0.13$, and $x = 0.19$ are used in the quantum well. Our buried quantum well design, compared to a surface layer, allows for more straightforward comparisons of the Rashba parameter between samples at nearly equal electric field and 2DEG density, as well as identification of electron scattering mechanisms over a broader range of 2DEG density.

Spin-orbit coupling and the resultant zero-field spin-split bands arises from broken inversion symmetry. Inversion asymmetry may be microscopic bulk inversion asymmetry (BIA) or structural inversion asymmetry (SIA). Dresselhaus SOC is associated with the lack of inversion symmetry in the crystal lattice, e.g., zinc-blende semiconductors [17]. The Rashba mechanism is due to asymmetry in the macroscopic potential induced by an external gate and/or an asymmetric heterostructure design [18]. In heterostructures built with small bandgap III-V zinc-blende semiconductors, the Rashba coupling is usually the dominant *k*-linear SOC term. Values for the Rashba parameter α for InSb and InAs quantum wells have been reported. Hatke *et al.* [19] reported $\alpha \approx 120$ meVÅ in deep InAs quantum wells at $n \approx 3 \times 10^{11}$ cm^{-2}; in modulation-doped InSb quantum wells Gilbertson *et al.* [20] extracted α between 130-160 meVÅ for a density range of $n \approx 3.15$-3.30×10^{11} cm^{-2}. We report Rashba coupling of $\alpha \approx 300$ meVÅ in a $InSb_{0.81}As_{0.19}$ quantum well, among the highest measured in III-V semiconductors [19–28].

II. EXPERIMENTAL DETAILS

We examine three heterostructures grown by molecular beam epitaxy (MBE) on GaAs (001) substrates with 0.5° miscut towards (111)*B*. Three different arsenic mole fractions are used in the $InSb_{1-x}As_x$ quantum well: $x = 0.05$, 0.13, and 0.19, labeled Sample A, B, and C respectively (see Table I). To mitigate lattice mismatch between the GaAs substrate and InSbAs quantum well and AlInSb barriers, the heterostructure [Fig. 1(a)] is built upon a relaxed buffer layer developed in

*Author to whom correspondence should be addressed: mmanfra@purdue.edu

TABLE I. Arsenic mole fraction, 2DEG density at zero gate bias, mobility at $n = 2.5 \times 10^{11}$ cm^{-2}, and effective mass extracted by temperature dependent SdH oscillations for the samples used in this study. Mobility is measured at $T = 0.3$ K.

	As mole fraction (x)	n at $V_g = 0$ V (10^{11} cm^{-2})	μ at $n = 2.5 \times 10^{11}$cm^{-2} (cm^2/Vs)	m* (m_e)
Sample A	0.05	0.6	2.4×10^5	0.0178 ± 0.0004
Sample B	0.13	1.4	2.0×10^5	0.0142 ± 0.0002
Sample C	0.19	2.3	1.4×10^5	0.0139 ± 0.0002

previous work [6,11]. The $InSb_{1-x}As_x$ quantum well is grown by keeping the In, Sb and As shutters open simultaneously; the arsenic mole fraction is determined by the substrate temperature and the Sb/As flux ratio. We utilize large-capacity cracker cells for group V elements (arsenic and antimony). All fluxes are measured with an ion gauge on the substrate manipulator prior to growth. The arsenic flux is also measured at completion of growth to ensure flux stability. Substrate temperature is monitored with a thermocouple in contact with the back side of the substrate, and additionally, we employ band edge optical thermometry.

Using a self-consistent Schrödinger-Poisson (SP) simulator (NEXTNANO^3 [29]) we calculate the band edge profile for the devices used in our experiments under changing gate potentials. As highlighted in Fig. 1(b), in comparison to undoped InSb quantum wells [28,30], these undoped InSbAs samples have a conductive 2DEG channel in the quantum well

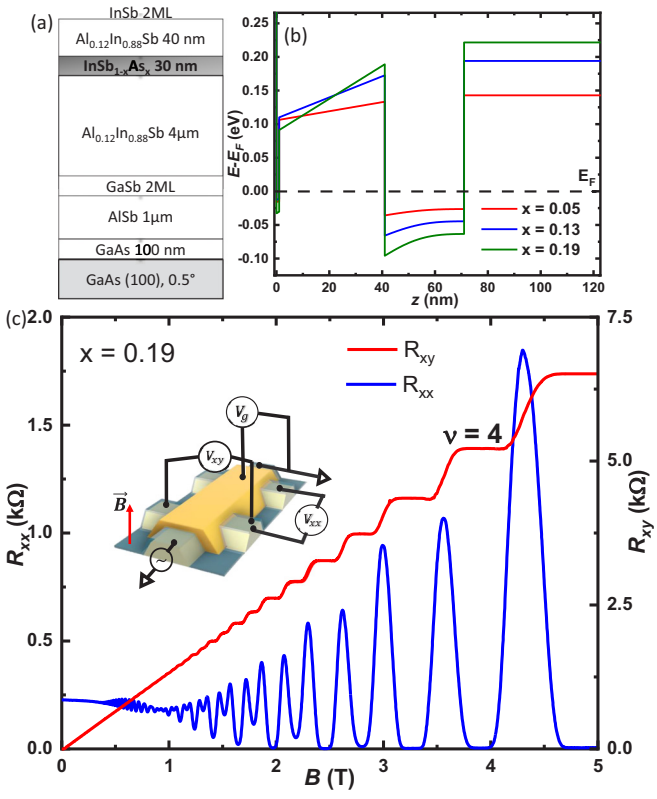

FIG. 1. (a) Schematic of the heterostructure used in this experiment. Arsenic mole fractions are $x = 0.05$, 0.13, and 0.19. (b) Band edge profile for $x = 0.05$, 0.13, and 0.19 at $V_g = 0$ V. (c) Magnetotransport measurement at $T = 0.3$ K of Sample C at $V_g = 0.65$ V with $n = 4.6 \times 10^{11}$ cm^{-2} and $\mu = 1.13 \times 10^5$ cm^2/Vs.

at zero gate bias; higher carrier density at $V_g = 0$ V is obtained with increasing arsenic mole fraction (see Table I) [11,31].

Insulated-gate Hall bars were fabricated to study electrical transport properties. Mesas were defined with a citric acid etch. The Hall bars typically are 75 μm wide and 1 mm long. The Ohmic probes are separated by 150 μm along the mesa edge. Before depositing the Ohmic metal stack an *in situ* argon ion mill with a voltage of 250 V, a beam current of 8 mA, and an accelerating voltage of 50 V was performed to etch the top barrier such that the contact metal stack is deposited directly at the InSbAs quantum well. Secondary ion mass spectroscopy was used to determine the position of the quantum well. This milling process was followed by deposition of 20 nm Ti and 180 nm Au for the Ohmic contacts. Next 40 nm of Al_2O_3 was deposited as a dielectric via atomic layer deposition at 100 °C. Finally, the gate electrodes were fabricated with the deposition of 20 nm of Ti and 150 nm Au.

Magnetotransport measurements were performed at temperatures between $T = 0.3$ K and $T = 10$ mK, unless otherwise specified. Higher temperature measurements were required for effective mass determination and investigation of magneto-intersubband scattering. In Fig. 1(c) we show representative high magnetic field data for Sample C. Well-defined integer quantum Hall states with vanishing longitudinal resistance and quantized Hall resistance are evident. The density calculated from the Hall slope matches the density extracted from analysis of Shubnikov de Haas (SdH) oscillations, indicative of a single conducting channel. We measured mobility as a function of 2DEG density for the three wafers at $T = 0.3$ K to identify the dominant scattering mechanisms and to observe changes that may occur as the arsenic mole fraction is varied between samples. For determination of SOC parameters, our analysis focused on high resolution low magnetic field ($B \leqslant 1$ T) measurements of the longitudinal resistance oscillations. We observe magnetoconductivity maxima around zero magnetic field (± 5 mT) attributed to weak antilocatization (WAL) and indicative of strong SOC [32]. Commonly used models of conductivity corrections due to WAL [32,33] in the diffusive limit are not reliable for our system due to its high mobility. Application of more elaborate models in the ballistic regime [34–36] are not pursued here.

III. RESULTS AND DISCUSSION

A. Electron scattering in ternary InSbAs quantum wells

Scattering of 2D electrons has been thoroughly investigated in the binary compounds InSb [28,37–40] and InAs [19,41]. It was determined that at cryogenic temperatures mobility is primarily limited by long-range Coulomb scattering from remote and background impurities for 2DEG

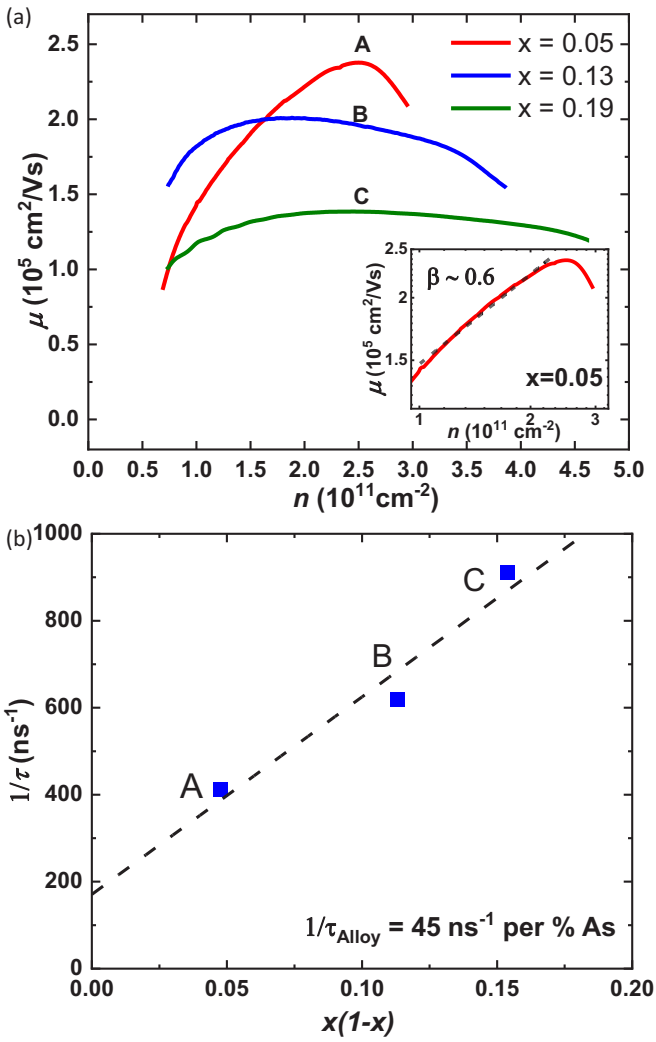

FIG. 2. (a) μ vs. 2DEG density measured at $T = 0.3$ K for Samples A, B, and C. Inset: μ vs. 2DEG density plotted in a log-log scale for Sample A and linear fit (dashed line) for extraction of β. (b) Total scattering rate $1/\tau$ vs $x(1-x)$ at $T = 0.3$ K and $n = 2.5 \times 10^{11}\text{cm}^{-2}$, where x is the arsenic mole fraction. The dashed line yields $1/\tau_{\text{alloy}} = 45\ \text{ns}^{-1}$ per % As.

densities below 1×10^{12} cm^{-2}. Here, we investigate mobility in ternary InSbAs quantum wells. A ternary quantum well may have additional sources of scattering. Anion atoms (Sb, As) will be randomly distributed based on the available sublattice sites, generating short-range disorder [42]. Alloy disorder and interface roughness scattering are sources of short-range scattering that may lower mobility and modify the functional dependence of mobility on 2DEG density in InSbAs channels [43,44].

Mobility (μ) vs. 2DEG density measured at T=0.3 K for different arsenic mole fractions is displayed in Fig. 2(a). As the arsenic mole fraction increases from Sample A to Sample C, a decrease in peak mobility is observed. In addition, a change in the functional dependence of μ vs. 2DEG density is evident. For Sample A at low density, mobility is a strongly increasing function of density, typical of charged impurity scattering. The dependence may be approximated by $\mu \propto n^{\beta}$ over the limited density range of $n = 1 - 2.2 \times 10^{11}\text{cm}^{-2}$, yielding an exponent of $\beta = 0.6$, as seen in the inset of Fig. 2(a) with data plotted on a log-log scale. $\beta = 0.6$ indicates that long-range charge disorder dominates scattering in this density regime, specifically Coulomb disorder near the quantum well [44]. In addition to point defects randomly distributed in the vicinity of the quantum well, the semiconductor/dielectric interface is a known source of fixed surface charge. In our structures, this surface is 40 nm away from the quantum well. Below $n = 1 \times 10^{11}\text{cm}^{-2}$, the slope in the μ vs. n data increases, suggestive of a transition to a localized regime at lowest density [44].

We note that at a fixed density of 2.5 $\times 10^{11}$ cm^{-2}, a decrease (increase) in mobility (scattering rate) with increasing arsenic mole fraction is observed, where $\mu = e\tau/m^*$. Mobility peaks at 2.4 $\times$ 10^5 cm^2/Vs for Sample A, followed by Sample B and Sample C with mobility of 2.0 $\times$ 10^5 cm^2/Vs and 1.4 $\times$ 10^5 cm^2/Vs at the same 2DEG density (Table I). A recent work from Lei *et al.* [28] reports mobility of 2.6 $\times$ 10^5 cm^2/Vs at density 2.4 $\times$ 10^{11} cm^{-2} in an undoped InSb quantum well, a value similar to that seen in Sample A, suggesting that alloy disorder scattering is not yet dominant at $x = 0.05$.

For Sample B and Sample C, the weaker dependence of mobility on 2DEG density suggests that short-range scattering limits mobility at increased arsenic mole fraction [44]. The progression of μ vs. n from Sample A to B and C indicates that alloy disorder significantly impacts mobility at mole fractions above $x = 0.05$.

According to Matthiessen's rule, the total scattering rate $(1/\tau)$ is determined by summing the scattering rates due to all independent scattering mechanisms. At fixed measurement temperature $T = 0.3$ K, we assume that $1/\tau = 1/\tau_{\text{other}} + 1/\tau_{\text{alloy}}$, where $1/\tau_{\text{other}}$ includes contributions for all scattering mechanisms other than alloy disorder scattering. The alloy scattering rate should be linear with $m^*[\delta V]^2 x(1-x)$, where x is the As mole fraction, m^* is the effective mass and $[\delta V]^2$ is the alloy scattering potential [45].

In order to assess the increase in scattering associated with the change in arsenic mole fraction we plot the total scattering rate $(1/\tau)$ vs $x(1-x)$ at $T = 0.3$ K and $n = 2.5 \times 10^{11}$ cm^{-2} as seen in Fig. 2(b). The linear dependence of the total scattering rate with $x(1-x)$ yields a slope of $1/\tau = 45\ \text{ns}^{-1}$ per % As, which quantifies the impact of alloy scattering as we increase arsenic mole fraction.

To the best of our knowledge, the alloy scattering rate in $InSb_{1-x}As_x$ quantum wells has not been reported previously. Therefore, we compare the extracted alloy scattering rate of $1/\tau_{\text{alloy}} = 45\ \text{ns}^{-1}$ per % As with the alloy scattering rate of $1/\tau_{\text{alloy}} = 24\ \text{ns}^{-1}$ per % As extracted by Gardner *et al.* [46] in the more widely studied $Al_xGa_{1-x}As$ ternary. The rate measured in $InSb_{1-x}As_x$ quantum wells is within a factor of 2 of $Al_xGa_{1-x}As$. $1/\tau_{\text{alloy}}$ is expected to be proportional to $[\delta V]^2$ and m*. The alloy scattering potential for the $InSb_{1-x}As_x$ alloy is theoretically predicted to be 0.82 eV compared to 0.12 eV for $Al_xGa_{1-x}As$ [47] while m^* is $\approx 0.010 - 0.019\text{m}_e$ for $InSb_{1-x}As_x$ ternary compared to 0.067m_e for $Al_xGa_{1-x}As$ [46]. Therefore, the alloy scattering rate for $InSb_{1-x}As_x$ is within a factor of 2 of $Al_xGa_{1-x}As$, despite the significantly higher alloy scattering potential,

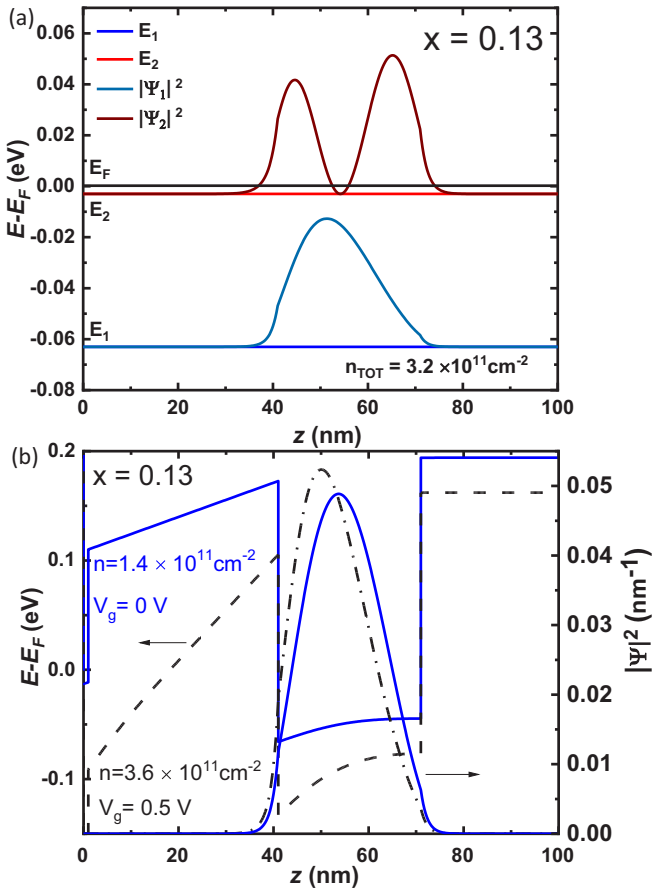

FIG. 3. (a) Self-consistent calculation of energy eigenvalues and wavefunctions of first and second subbands, when total density $n = 3.2 \times 10^{11}$ cm^{-2}. (b) Self-consistent calculation of band diagram and wavefunction of the first subband at $V_g = 0$ V, with density $n = 1.4 \times 10^{11}$ cm^{-2} (Solid line) and at $V_g = 0.5$ V with density $n = 3.6 \times 10^{11}$ cm^{-2} (Dashed line). As the gate voltage increases, we observe enhanced band bending and asymmetry of the wavefunction within the quantum well.

due to the compensatory impact of the lower effective mass.

We performed temperature dependent magnetotransport measurements to extract the values of the effective mass for all samples at a density of $n \approx 2 \times 10^{11}$ cm^{-2} [48]. Theory and experiments have shown that the ternary $InSb_{1-x}As_x$ has a lower effective mass with increasing arsenic mole fraction [11,13,14,31]. Our analysis yielded results consistent with this trend, as displayed in Table I.

Finally, we note a decrease in mobility for all samples above $n \approx 2.5 \times 10^{11}$ cm^{-2}, as seen Fig. 2(a). Simulations point to the occupation of the second subband at a similar density for all samples, $n \approx 3 \times 10^{11}$ cm^{-2}, as seen in Fig. 3(a). The drop in mobility in our data may be attributed to the proximity of the Fermi level to the bottom of the second subband, allowing a channel for intersubband scattering [49]. Another possible contribution is interface roughness scattering, since the electron wavefuncion is pulled closer to the top barrier with higher gate voltage, as seen in the simulation shown in Fig. 3(b).

B. Analysis of spin-orbit coupling in InSbAs quantum wells

Due to high mobility and small effective mass we are able to resolve beating in the oscillatory longitudinal resistance at low magnetic field. Beating may be driven by several mechanisms, including density inhomogeneity [50], magneto-intersubband scattering [51–54] or zero-field spin splitting arising from strong spin-orbit coupling [55]. Magnetotransport measurements taken with different contact configurations on our devices indicate that beating does not result from density inhomogeneity. Intersubband scattering may occur when the chemical potential is proximal to the second electric subband. Landau level crossing enhances magneto-intersubband scattering at magnetic field given by $B_{\mathrm{MIS}} = (\Delta E_{1,2} m^*)/(e\hbar)$ [51–54]. As noted previously, simulations indicate the occupation of the second subband is possible at high 2DEG density, therefore we have measured temperature-dependent magnetotransport to rule out magneto-intersubband scattering.

We first note that the magnetotransport does not show signs of significant parasitic conduction. As shown in Fig. 1(b), clear quantum Hall plateaus are resolved with the longitudinal resistance vanishing at 1.8 T. Furthermore, the densities extracted from the Hall slope and from the SdH oscillation minima are equal. This suggests minimal contribution from parallel conduction channels in the investigated range of density, with only the lowest energy subband contributing significantly to transport.

Magneto-intersubband scattering occurs when the Landau levels of two bands cross, causing oscillations in the magnetotransport at frequency $B_{\mathrm{MIS}} = (\Delta E_{1,2} m^*)/(e\hbar)$. If this value is close to the frequency of the underlying SdH oscillations, beating may result. To understand if this mechanism was active in our devices, measurements of the longitudinal resistance were performed over a broad range of temperature. Magneto-intersubband scattering is relatively insensitive to changes in temperature, whereas damping of the SdH oscillations with temperature occurs rapidly as $A(T) \propto x/\sinh(x)$ with $x = (2\pi^2 k_b T/\hbar\omega_c)$ where $\omega_c = eB/m^*$ [27,53,54]. We performed temperature dependent measurements for Sample B and Sample C at the highest achievable density. We observe rapid damping of the oscillations [Fig. 4(a)] with increased temperature, also reflected in the fast Fourier transforms (FFT). The amplitudes of the two frequency peaks clearly decrease with increasing temperature [Fig. 4(b)], indicating that their origin is SdH oscillations rather than magneto-intersubband scattering.

C. Rashba spin-orbit coupling

The beating observed in low-field transport in our samples is attributed to zero-field spin-splitting due to strong Rashba spin-orbit coupling. Zero-field spin-splitting (Δ_{so}) is given by $2\alpha k_F$, where k_F is the Fermi wave vector defined as $k_F = \sqrt{2\pi n}$ and α is the Rashba coupling parameter. The presence of SOC results in beating in the SdH oscillations as seen in Fig. 5. Beating occurs because two occupied spin bands have two slightly different densities of electrons, giving rise to two closely spaced frequencies of SdH oscillations. This allows extraction of α from oscillatory low-field transport [19,21,23,56–58]. Fourier analysis of longitudinal

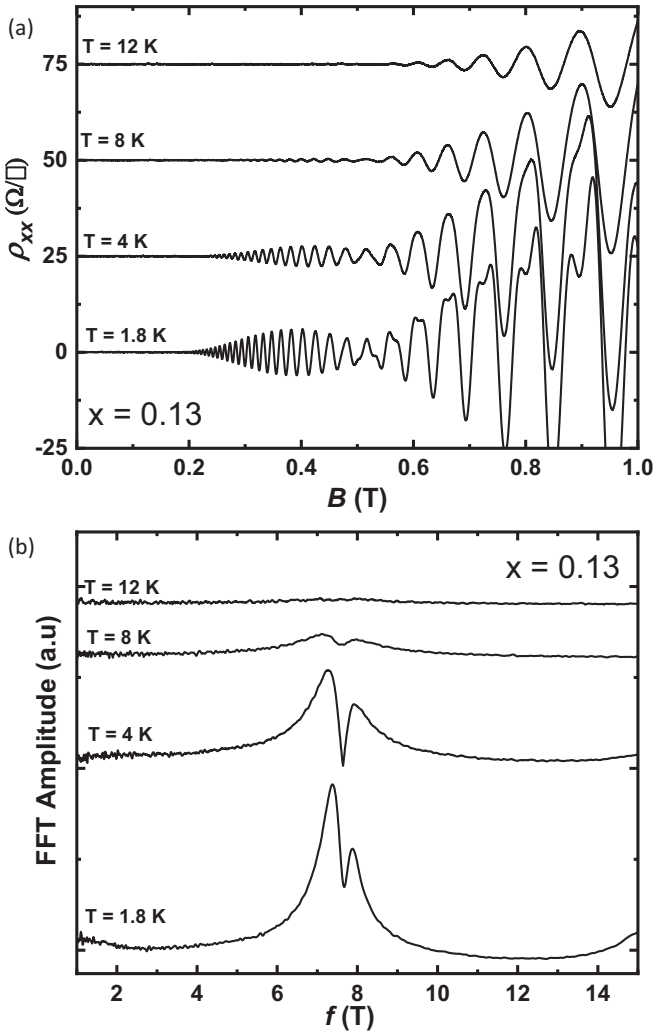

FIG. 4. (a) Magnetotransport as a function of temperature for $x = 0.13$ at density of $n = 3.6 \times 10^{11}$ cm^{-2}. (b) Fast Fourier transforms for the data shown in a). The damping of the FFT peaks as a function of temperature indicates that the peaks are generated by SdH oscillations and not by magneto-intersubband scattering.

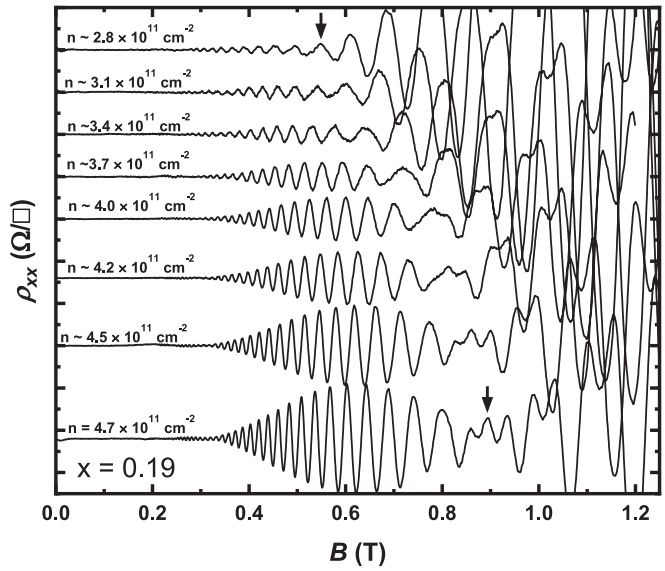

FIG. 5. SdH oscillations as a function of density for $x = 0.19$. A shift of the 2nd node to higher magnetic field is observed as the density increases.

magnetoresistance facilitates extraction of the Rashba parameter α as a function of 2DEG density and arsenic mole fraction in our devices.

We assume the Rashba coupling is the major contribution to SOC in our devices. Due to the lack of microscopic inversion symmetry in zinc-blende crystals, the k^3 Dresselhaus coupling also contributes to SOC in zinc-blende InSbAs quantum wells [25,59]. However, Rashba coupling is known to dominate in highly asymmetric quantum wells such as those studied here [20,60]. The increased electrostatic asymmetry with increased gate voltage is confirmed by self-consistent calculation of the band diagram as shown in Fig. 3(b).

The Rashba parameter depends on the electric field in the quantum well and in the top and bottom barriers when the wavefunction has finite value in the barriers. The conduction band discontinuities at the top and bottom interfaces also contribute when the wavefunction has differing amplitude at the top and bottom interfaces [57,58].

$$\alpha \propto a_0 \bar{E}_{QW} + b'(\bar{E}_u + \bar{E}_l) - b(|\Psi_u|^2 - |\Psi_l|^2). \quad (1)$$

The parametric dependence of α is shown in Eq. (1), where the first term is the average value of the electric field in the quantum well ($\bar{E}_{QW}$) weighted by a_0, a material specific parameter determined by interband matrix elements and energy differences [61]. a_0 is expected to increase with increasing arsenic mole fraction in the InSbAs ternaries we study. The second term contains the average value of the electric field in the upper ($\bar{E}_u$) and lower ($\bar{E}_l$) barriers weighted by b' which characterizes Rashba coupling in the barriers. The third term accounts for the contributions from the wavefunction at the upper ($|\Psi_u|^2$) and lower interface ($|\Psi_l|^2$), where b parameterizes band discontinuity at the interfaces.

The Rashba parameter is determined once Δn, the density difference between the two electron spin bands, is known [57]. This is accomplished by taking a fast Fourier transform of the low-field longitudinal resistance, which yields the frequencies of the two oscillations, f_1 and f_2. The Rashba parameter is given by Eq. (2) [57]:

$$\alpha = \frac{\Delta n \hbar^2}{m^*} \sqrt{\frac{\pi}{2(n_{\text{tot}} - \Delta n)}}. \quad (2)$$

In Eq. (2), $n_{\text{tot}} = n_1 + n_2$, $\Delta n = n_1 - n_2$, and m^* is the effective mass. We use the effective mass values measured for our samples as shown in Table I.

The increase of the Rashba coupling with larger arsenic mole fraction is evident in the raw magnetoresistance data plotted in Fig. 6(a). The number of oscillations between two nodes changes from approximately 25 to 13, from $x = 0.13$ to $x = 0.19$. Since the number of oscillations is inversely proportional to Δ_{so}, this indicates a higher α for the higher arsenic mole fraction sample [21,55]. The evolution of the Rashba parameter with density for all arsenic mole fractions is depicted in Fig. 6(b). A noticeable increase of the Rashba

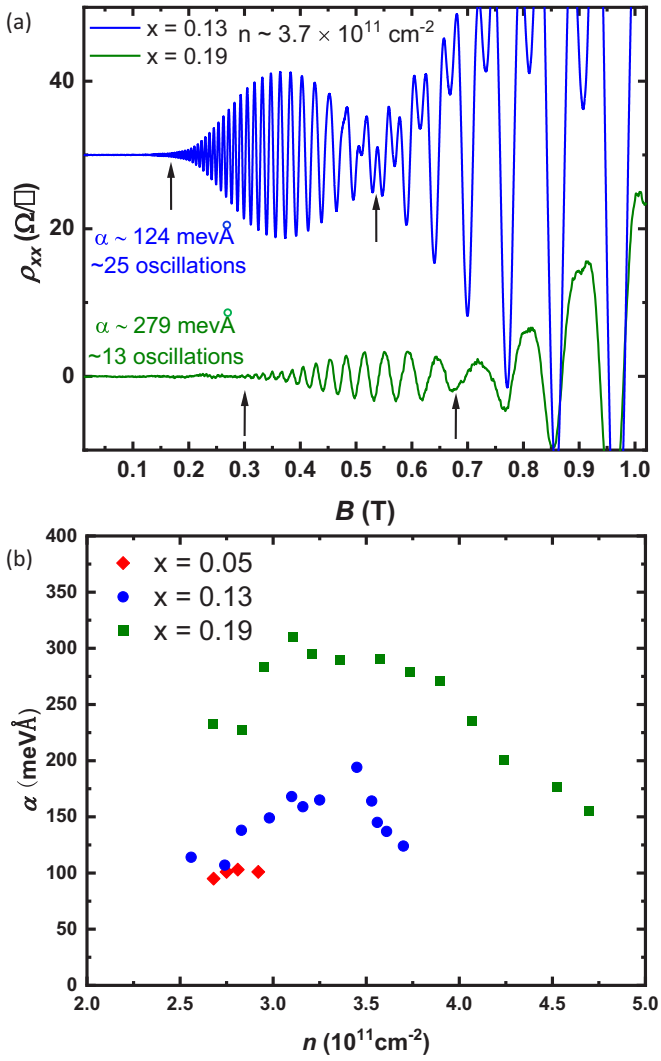

FIG. 6. (a) Direct comparison of beating in SdH oscillations with $x = 0.13$ and $x = 0.19$ at $n = 3.7 \times 10^{11}$ cm^{-2}. Comparison at the same density allows for comparison at similar electric field. The number of oscillations between two nodes is inversely proportional to the value of Δ_{so}. For $x = 0.13$ we observe a larger number of oscillations compared to $x = 0.19$, confirming a lower value of zero-field spin splitting energy. (b) Extracted Rashba parameter as a function of 2DEG density for all samples.

coupling with increased arsenic mole fraction is evident. If we compare the Rashba coupling extracted at the same density, $n \approx 2.9 \times 10^{11}$ cm^{-2}, the values for Sample A to C are respectively $\alpha \approx 100$, 150, and 280 meVÅ. Because the samples have the same top and bottom barriers, nearly equal electric field in the quantum well, and matching electron distributions (as inferred from simulations), the increase in SOC may be attributed to an increase in the material specific Rashba coupling parameter a_0 with higher arsenic concentration. This is consistent with predictions [8,13–15], in which the Rashba parameter increases with arsenic mole fraction up to $x \approx 0.5 \sim 0.6$ and then decreases towards the value of binary InAs. In recent work using an $InSb_{0.5}As_{0.5}$ surface layer at $n = 8 \times 10^{11}$ cm^{-2}, Mayer *et al.* [8] measured a Rashba parameter of 800 meVÅ, also significantly higher than the value of InAs and InSb. However, a direct comparison with our samples is nontrivial since the electric field, density, and heterostructure are significantly different.

For Sample B and Sample C, the Rashba coupling increases from $n \approx 2.5$ and 3.5×10^{11} cm^{-2}. This enhancement is consistent with simulations, which indicate an increase in electric field and wavefunction asymmetry towards the top barrier, as also seen in Fig. 3(b). However, for both Samples B and C, the Rashba parameter decreases after $n \approx 3.5 \times 10^{11}$ cm^{-2}. It is worth noting that the decrease in α occurs at approximately the same density at which the second electric subband begins to be occupied in the numerical simulations, although contribution from a second subband to the magnetotransport is not apparent in the data. From the simulations, the second subband wavefunction penetrates significantly more into the top barrier than the first subband. A possible explanation for the decrease in α with higher density is the increased propensity of electrons to reside in the top barrier, which has lower intrinsic SOC than the quantum well. However, more investigation is needed to quantitatively understand this trend.

IV. CONCLUSIONS

In this work we have detailed the low temperature transport properties of a series of 2DEGs confined in InSbAs quantum wells with different arsenic mole fractions. We extracted an alloy scattering rate of $1/\tau = 45$ ns^{-1} per % As, determined the dependence of mobility on 2DEG density and arsenic mole fraction, and detailed the evolution of dominant scattering mechanisms. Analysis of SdH oscillations enabled extraction of the Rashba coupling strength over a wide range of 2DEG density for all mole fractions. At comparable density and nearly equal electric field, we observed an increase of α with arsenic mole fraction. For $x = 0.19$, α is ≈ 300 meVÅ, one of the highest values reported for III-V heterostructures. These results agree with theoretical predictions of enhancement of SOC with arsenic mole fraction [13–15] and suggest that $InSb_{1-x}As_x$ 2DEGs are a promising platform for exploration of topological superconductivity by incorporating these ternary quantum wells in a shallow structure coupled to an *s*-wave superconductor.

The data that support the findings of this study are available from the corresponding author upon reasonable request.

ACKNOWLEDGMENTS

We thank Dr. J. Nakamura for manuscript improvement suggestions and G. Winkler, S. Teicher, and F. Corsetti for fruitful discussion. This work was supported by Microsoft Quantum.

The authors have no conflicts to disclose.

[1] R. M. Lutchyn, J. D. Sau, and S. D. Sarma, Majorana Fermions and a Topological Phase Transition in Semiconductor-Superconductor Heterostructures, Phys. Rev. Lett. **105**, 077001 (2010).

[2] Y. Oreg, G. Refael, and F. von Oppen, Helical Liquids and Majorana Bound States in Quantum Wires, Phys. Rev. Lett. **105**, 177002 (2010).

[3] J. Shabani, M. Kjaergaard, H. J. Suominen, Y. Kim, F. Nichele, K. Pakrouski, T. Stankevic, R. M. Lutchyn, P. Krogstrup, R. Feidenhans'l, S. Kraemer, C. Nayak, M. Troyer, C. M. Marcus, and C. J. Palmstrøm, Two-dimensional epitaxial superconductor-semiconductor heterostructures: A platform for topological superconducting networks, Phys. Rev. B **93**, 155402 (2016).

[4] M. Kjaergaard, F. Nichele, H. J. Suominen, M. P. Nowak, M. Wimmer, A. R. Akhmerov, J. A. Folk, K. Flensberg, J. Shabani, C. J. Palmstrøm, and C. M. Marcus, Quantized conductance doubling and hard gap in a two-dimensional semiconductor-superconductor heterostructure, Nat. Commun. **7**, 12841 (2016).

[5] A. C. C. Drachmann, H. J. Suominen, M. Kjaergaard, B. Shojaei, C. J. Palmstrøm, C. M. Marcus, and F. Nichele, Proximity Effect Transfer from NbTi into a Semiconductor Heterostructure via Epitaxial Aluminum, Nano Lett. **17**, 1200 (2017).

[6] C. T. Ke, C. M. Moehle, F. K. de Vries, C. Thomas, S. Metti, C. R. Guinn, R. Kallaher, M. Lodari, G. Scappucci, T. Wang, R. E. Diaz, G. C. Gardner, M. J. Manfra, and S. Goswami, Ballistic superconductivity and tunable π-junctions in InSb quantum wells, Nat. Commun. **10**, 3764 (2019).

[7] A. Fornieri, A. M. Whiticar, F. Setiawan, E. Portolés, A. C. Drachmann, A. Keselman, S. Gronin, C. Thomas, T. Wang, R. Kallaher *et al.*, Evidence of topological superconductivity in planar Josephson junctions, Nature (London) **569**, 89 (2019).

[8] W. Mayer, W. F. Schiela, J. Yuan, M. Hatefipour, W. L. Sarney, S. P. Svensson, A. C. Leff, T. Campos, K. S. Wickramasinghe, Dartiailh *et al.*, Superconducting proximity effect in InAsSb surface quantum wells with in situ Al contacts, ACS Appl. Electron. Mater. **2**, 2351 (2020).

[9] M. C. Dartiailh, J. J. Cuozzo, B. H. Elfeky, W. Mayer, J. Yuan, K. S. Wickramasinghe, E. Rossi, and J. Shabani, Missing Shapiro steps in topologically trivial Josephson junction on InAs quantum well, Nat. Commun. **12**, 78 (2021).

[10] M. C. Dartiailh, W. Mayer, J. Yuan, K. S. Wickramasinghe, A. Matos-Abiague, I. Žutić, and J. Shabani, Phase Signature of Topological Transition in Josephson Junctions, Phys. Rev. Lett. **126**, 036802 (2021).

[11] C. M. Moehle, C. T. Ke, Q. Wang, C. Thomas, D. Xiao, S. Karwal, M. Lodari, V. van de Kerkhof, R. Termaat, G. C. Gardner, G. Scappucci, M. J. Manfra, and S. Goswami, InSbAs two-dimensional electron gases as a platform for topological superconductivity, Nano Lett. **21**, 9990 (2021).

[12] S. Datta and B. Das, Electronic analog of the electro-optic modulator, Appl. Phys. Lett. **56**, 665 (1990).

[13] O. Berolo, J. C. Woolley, and J. A. Van Vechten, Effect of disorder on the conduction-band effective mass, valence-band spin-orbit splitting, and the direct band gap in III-V alloys, Phys. Rev. B **8**, 3794 (1973).

[14] N. Bouarissa and H. Aourag, Effective masses of electrons and heavy holes in InAs, InSb, GaSb, GaAs and some of their ternary compounds, Infrared Phys. Technol. **40**, 343 (1999).

[15] G. W. Winkler, Q. S. Wu, M. Troyer, P. Krogstrup, and A. A. Soluyanov, Topological Phases in $InAs_{1-x}Sb_x$: From Novel Topological Semimetal to Majorana Wire, Phys. Rev. Lett. **117**, 076403 (2016).

[16] J. E. Sestoft, T. Kanne, A. N. Gejl, M. Von Soosten, J. S. Yodh, D. Sherman, B. Tarasinski, M. Wimmer, E. Johnson, M. Deng, J. Nygård, T. S. Jespersen, C. M. Marcus, and P. Krogstrup, Engineering hybrid epitaxial InAsSb/Al nanowires for stronger topological protection, Phys. Rev. Mater. **2**, 044202 (2018).

[17] G. Dresselhaus, Spin-orbit coupling effects in zinc blende structures, Phys. Rev. **100**, 580 (1955).

[18] Y. A. Bychkov and E. I. Rashba, Oscillatory effects and the magnetic susceptibility of carriers in inversion layers, J. Phys. C: Solid State Phys. **17**, 6039 (1984).

[19] A. T. Hatke, T. Wang, C. Thomas, G. C. Gardner, and M. J. Manfra, Mobility in excess of 10^6 cm^2/Vs in InAs quantum wells grown on lattice mismatched InP substrates, Appl. Phys. Lett. **111**, 142106 (2017).

[20] A. M. Gilbertson, W. R. Branford, M. Fearn, L. Buckle, P. D. Buckle, T. Ashley, and L. F. Cohen, Zero-field spin splitting and spin-dependent broadening in high-mobility $InSb/In_{1-x}Al_xSb$ asymmetric quantum well heterostructures, Phys. Rev. B **79**, 235333 (2009).

[21] J. Nitta, T. Akazaki, H. Takayanagi, and T. Enoki, Gate Control of Spin-Orbit Interaction in an Inverted $In_{0.53}Ga_{0.47}As/In_{0.52}Al_{0.48}As$ Heterostructure, Phys. Rev. Lett. **78**, 1335 (1997).

[22] J. Luo, H. Munekata, F. F. Fang, and P. J. Stiles, Effects of inversion asymmetry on electron energy band structures in GaSb/InAs/GaSb quantum wells, Phys. Rev. B **41**, 7685 (1990).

[23] J. P. Heida, B. J. van Wees, J. J. Kuipers, T. M. Klapwijk, and G. Borghs, Spin-orbit interaction in a two-dimensional electron gas in a InAs/AlSb quantum well with gate-controlled electron density, Phys. Rev. B **57**, 11911 (1998).

[24] K.-H. Kim, H.-J. Kim, H. C. Koo, J. Chang, and S.-H. Han, Spin-Orbit coupling in double-sided dopes InAs quantum well structures, Appl. Phys. Lett. **97**, 012504 (2010).

[25] R. L. Kallaher, J. J. Heremans, N. Goel, S. J. Chung, and M. B. Santos, Spin-orbit interaction determined by antilocalization in an InSb quantum well, Phys. Rev. B **81**, 075303 (2010).

[26] T. Y. Lee, J. Chang, M. C. Hickey, H. C. Koo, H.-J. Kim, S. H. Han, and J. S. Moodera, Quantum well thickness dependence of Rashba spin-orbit coupling in the InAs/InGaAs heterostructure, Appl. Phys. Lett. **98**, 202504 (2011).

[27] B. Shojaei, P. J. J. O'Malley, J. Shabani, P. Roushan, B. D. Schultz, R. M. Lutchyn, C. Nayak, J. M. Martinis, and C. J. Palmstrøm, Demonstration of gate control of spin splitting in a high-mobility InAs/AlSb two-dimensional electron gas, Phys. Rev. B **93**, 075302 (2016).

[28] Z. Lei, E. Cheah, K. Rubi, M. E. Bal, C. Adam, R. Schott, U. Zeitler, W. Wegscheider, T. Ihn, and K. Ensslin, High-quality two-dimensional electron gas in undoped InSb quantum wells, Phys. Rev. Res. **4**, 013039 (2022).

[29] S. Birner, T. Zibold, T. Andlauer, T. Kubis, M. Sabathil, A. Trellakis, and P. Vogl, Nextnano: General purpose 3-D simulations, IEEE Trans. Electron Dev **54**, 2137 (2007).

[30] I. Kulesh, C. T. Ke, C. Thomas, S. Karwal, C. M. Moehle, S. Metti, R. Kallaher, G. C. Gardner, M. J. Manfra, and S. Goswami, Quantum Dots in an InSb Two-Dimensional Electron Gas, Phys. Rev. Appl. **13**, 041003 (2020).

[31] S. Suchalkin, J. Ludwig, G. Belenky, B. Laikhtman, G. Kipshidze, Y. Lin, L. Shterengas, D. Smirnov, S. Luryi, W. L. Sarney, and S. P. Svensson, Electronic properties of unstrained unrelaxed narrow gap $InAs_xSb_{1-x}$ alloys, J. Phys. D: Appl. Phys. **49**, 105101 (2016).

[32] W. Knap, C. Skierbiszewski, A. Zduniak, E. Litwin-Staszewska, D. Bertho, F. Kobbi, J. L. Robert, G. E. Pikus, F. G. Pikus, S. V. Iordanskii, V. Mosser, K. Zekentes, and Y. B. Lyanda-Geller, Weak antilocalization and spin precession in quantum wells, Phys. Rev. B **53**, 3912 (1996).

[33] S. Hikami, A. I. Larkin, and Y. Nagaoka, Spin-orbit interaction and magnetoresistance in the two dimensional random system, Prog. Theor. Phys. **63**, 707 (1980).

[34] J. B. Miller, D. M. Zumbühl, C. M. Marcus, Y. B. Lyanda-Geller, D. Goldhaber-Gordon, K. Campman, and A. C. Gossard, Gate-Controlled Spin-Orbit Quantum Interference Effects in Lateral Transport, Phys. Rev. Lett. **90**, 076807 (2003).

[35] M. M. Glazov and L. E. Golub, Spin-orbit interaction and weak localization in heterostructures, Semicond. Sci. Technol. **24**, 064007 (2009).

[36] Y. Lyanda-Geller, Quantum Interference and Electron-Electron Interactions at Strong Spin-Orbit Coupling in Disordered Systems, Phys. Rev. Lett. **80**, 4273 (1998).

[37] S. J. Chung, K. J. Goldammer, S. C. Lindstrom, M. B. Johnson, and M. B. Santos, Study of factors limiting electron mobility in InSb quantum wells, J. Vacuum Sci. Tech. B: Microelec. Nanometer Struct. Proc. Measure. Phenomena **17**, 1151 (1999).

[38] W. Yi, A. A. Kiselev, J. Thorp, R. Noah, B.-M. Nguyen, S. Bui, R. D. Rajavel, T. Hussain, M. F. Gyure, P. Kratz, Q. Qian, M. J. Manfra, V. S. Pribiag, L. P. Kouwenhoven, C. M. Marcus, M. Sokolich, W. Yi, A. A. Kiselev, J. Thorp, R. Noah *et al.*, Gate-tunable high mobility remote-doped $InSb/In_{1-x}Al_xSb$ quantum well heterostructures, Appl. Phys. Lett. **106**, 142103 (2015).

[39] O. Pooley, A. Gilbertson, P. D. Buckle, R. Hall, M. Emeny, M. Fearn, M. Halsall, L. Cohen, and T. Ashley, Quantum well mobility and the effect of gate dielectrics in remote doped $InSb/Al_xIn_{1-x}Sb$ heterostructures, Semicond. Sci. Technol. **25**, 125005 (2010).

[40] C. A. Lehner, T. Tschirky, T. Ihn, W. Dietsche, J. Keller, S. Fält, and W. Wegscheider, Limiting scattering processes in high-mobility InSb quantum wells grown on GaSb buffer systems, Phys. Rev. Mater. **2**, 054601 (2018).

[41] J. Shabani, A. P. McFadden, B. Shojaei, and C. J. Palmstrøm, Gating of high-mobility InAs metamorphic heterostructures, Appl. Phys. Lett. **105**, 262105 (2014).

[42] J. Harrison and J. Hauser, Alloy scattering in ternary III-V compounds, Phys. Rev. B **13**, 5347 (1976).

[43] V. W. Chin, R. Egan, and T. Tansley, Electron mobility in $InAs_{1-x}Sb_x$ and the effect of alloy scattering, J. Appl. Phys. **69**, 3571 (1991).

[44] S. Das Sarma and E. H. Hwang, Universal density scaling of disorder-limited low-temperature conductivity in high-mobility two-dimensional systems, Phys. Rev. B **88**, 035439 (2013).

[45] G. Bastard, *Wave mechanics applied to semiconductor heterostructures* (New York, Wiley-Interscience, 1991).

[46] G. C. Gardner, J. D. Watson, S. Mondal, N. Deng, G. A. Csáthy, and M. J. Manfra, Growth and electrical characterization of $Al_{0.24}Ga_{0.76}As/Al_xGa_{1-x}as/Al_{0.24}Ga_{0.76}As$ modulation-doped quantum wells with extremely low x, Appl. Phys. Lett. **102**, 252103 (2013).

[47] D. K. Ferry, Alloy Scattering in ternary III-V compound, Phys. Rev. B **17**, 912 (1978).

[48] T. Ihn, *Semiconductor Nanostructures: Quantum States and Electronic Transport* (Oxford University Press, Oxford, 2010)

[49] R. Fletcher, E. Zaremba, M. O'iorio, C. T. Foxon, and J. J. Harris, Evidence of a mobility edge in the second subband of an $Al_{0.33}Ga_{0.67}As$-GaAs heterojunction, Phys. Rev. B **38**, 7866(R) (1988).

[50] S. Brosig, K. Ensslin, R. J. Warburton, C. Nguyen, B. Brar, M. Thomas, and H. Kroemer, Zero-field spin splitting in InAs − AlSb quantum wells revisited, Phys. Rev. B **60**, R13989(R) (1999).

[51] D. R. Leadley, R. Fletcher, R. J. Nicholas, F. Tao, C. T. Foxon, and J. J. Harris, Intersubband resonant scattering in GaAs-$Ga_{1-x}Al_xAs$ heterojunctions, Phys. Rev. B **46**, 12439 (1992).

[52] M. E. Raikh and T. V. Shahbazyan, Magnetointersubband oscillations of conductivity in a two-dimensional electronic system, Phys. Rev. B **49**, 5531 (1994).

[53] T. H. Sander, S. N. Holmes, J. J. Harris, D. K. Maude, and J. C. Portal, Determination of the phase of magneto-intersubband scattering oscillations in heterojunctions and quantum wells, Phys. Rev. B **58**, 13856 (1998).

[54] A. C. H. Rowe, J. Nehls, R. A. Stradling, and R. S. Ferguson, Origin of beat patterns in the quantum magnetoresistance of gated InAs/GaSb and InAs/AlSb quantum wells, Phys. Rev. B **63**, 201307(R) (2001).

[55] J. Luo, H. Munekata, F. F. Fang, and P. J. Stiles, Observation of the zero-field spin splitting of the ground electron subband in GaSb − InAs − GaSb quantum wells, Phys. Rev. B **38**, 10142(R) (1988).

[56] B. Das, D. C. Miller, S. Datta, R. Reifenberger, W. P. Hong, P. K. Bhattacharya, J. Singh, and M. Jaffe, Evidence for spin splitting in $In_xGa_{1-x}As/In_{0.52}Al_{0.48}As$ heterostructures as $B \rightarrow 0$, Phys. Rev. B **39**, 1411(R) (1989).

[57] G. Engels, J. Lange, T. Schäpers, and H. Lüth, Experimental and theoretical approach to spin splitting in modulation-doped $In_xGa_{1-x}As/$ InP quantum wells for $B \rightarrow 0$, Phys. Rev. B **55**, R1958(R) (1997).

[58] T. Schäpers, G. Engels, J. Lange, T. Klocke, M. Hollfelder, and H. Lüth, Effect of the heterointerface on the spin splitting in modulation doped $In_xGa_{1-x}As/InP$ quantum wells for $B \rightarrow 0$, J. Appl. Phys. **83**, 4324 (1998).

[59] N. Nishizako, T. Manago, S. Ishida, H. Geka, and I. Shibasaki, Carrier density dependence of spin-orbit interaction in InAsSb quantum wells, Phys. E **42**, 975 (2010).

[60] G. A. Khodaparast, R. E. Doezema, S. J. Chung, K. J. Goldammer, and M. B. Santos, Spectroscopy of Rashba spin splitting in InSb quantum wells, Phys. Rev. B **70**, 155322 (2004).

[61] R. Winkler, *Spin-orbit coupling effects in two-dimensional electron and hole systems* (Springer, 2003), Vol. 191.